Available online at www.sciencedirect.com
ScienceDirect
Acta Materialia 55 (2007) 6541–6552
Acta MATERIALIA
www.elsevier.com/locate/actamat

Mode I crack tip fields in amorphous materials with application to metallic glasses

Parag Tandaiya [a], R. Narasimhan [a], U. Ramamurty [b,*]

[a] Department of Mechanical Engineering, Indian Institute of Science, Bangalore 560 012, India
[b] Department of Materials Engineering, Indian Institute of Science, Bangalore 560 012, India

Received 17 May 2007; received in revised form 3 August 2007; accepted 6 August 2007
Available online 4 October 2007

Abstract

In this work, stationary crack tip fields in amorphous materials such as metallic glasses under mode I loading are studied to understand the factors that control crack tip plasticity and in turn impart toughness to those materials. For this purpose, finite element simulations under plane strain, small scale yielding conditions are performed. A continuum elastic–viscoplastic constitutive theory, which accounts for pressure sensitivity of plastic flow as well as the localization of plastic strain into discrete shear bands, is employed to represent the material behavior. The influence of internal friction and strain softening on the plastic zone, stress and deformation fields and notch opening profile is examined. It is found that higher internal friction leads to a larger plastic zone. Also, it enhances the plastic strain ahead of the notch tip but leads to a substantial decrease in the opening stress. Thus, it appears that a higher friction parameter promotes toughening of amorphous solids. The shear band patterns within the plastic zone and brittle crack trajectories around the notch root generated from the simulations match qualitatively with those observed in experiments.

Keywords: Bulk amorphous materials; Metallic glasses; Mode I crack tip fields; Finite element analysis; Shear bands

1. Introduction

Bulk metallic glasses (BMGs) represent a relatively young class of structural materials with an impressive combination of mechanical properties. Indeed, extremely high strengths coupled with reasonable toughness of these materials has led to substantial recent research effort with emphasis on the underlying deformation physics in them [1]. In spite of their intrinsic inability to undergo extensive plastic straining under tension, some of the metallic glasses do exhibit good toughness values, whereas others are quite brittle. Despite the importance of this issue for widespread structural usage of metallic glasses, their fracture behavior has received relatively little attention. This work was undertaken to develop detailed understanding of the fracture mechanics and mechanisms in amorphous solids, especially the development of the plastic zone ahead of the crack tip and the material parameters that control it. In this paper, results of finite element simulations of mode I loading of a crack in an amorphous material under plane strain, small scale yielding (SSY) conditions are reported. The constitutive behavior is represented by the model developed by Anand and Su [2], which accounts for pressure sensitivity of plastic flow as well as the localization of plastic strain into discrete shear bands typically exhibited by metallic glasses. Although this study pays specific attention to fracture in amorphous alloys, many of the observations made and implications drawn from this study are equally applicable to other amorphous materials such as glassy polymers.

2. Background

The inelastic deformation of amorphous materials such as BMGs, glassy polymers and ceramics is fundamentally

* Corresponding author. Tel.: +91 80 2293 3241; fax: +91 80 2360 0472.
E-mail address: ramu@materials.iisc.ernet.in (U. Ramamurty).

1359-6454/$30.00
doi:10.1016/j.actamat.2007.08.017

different from that of crystalline metals. At a microscopic level, for temperatures below the glass transition temperature, the inelastic deformation in metallic glasses occurs by local shearing of clusters of atoms, referred to as shear transformation zones, in regions having high free-volume. This shearing is accompanied by inelastic dilatation that causes strain softening [3], which then leads to localization of plastic strain into discrete shear bands. Similarly, yielding in glassy polymers and ceramics is sensitive to hydrostatic stress [4,5] and is accompanied by plastic dilatation. Further, the yield stress under uniaxial tension for amorphous materials is different from that in uniaxial compression (see, for example, [6,7]). It has also been observed that, in these materials, the shear bands depart from the plane of maximum shear stress [7].

Several constitutive models have been proposed in the literature (see e.g. Refs. [6–9]) to describe the yield behavior of metallic glasses and polymers. Experiments and molecular dynamics simulations on BMGs [7,10] indicate that the normal as well as shear stress acting on the slip plane influences their yield behavior, which is accurately captured by the Mohr–Coulomb yield criterion. This is also true of glassy polymers exhibiting plastic flow by discrete shear banding, such as polystyrene and polyethylene terephthalate [4,6]. In this connection, it must be mentioned that the Mohr–Coulomb based constitutive model proposed recently by Anand and Su (AS) [2] is capable of representing inhomogeneous deformation by discrete shear banding.

Over the last decade, some experimental research has been undertaken to characterize the fracture response of metallic glasses. Fracture toughness values ranging from as low as 2 MPa $\sqrt{\mathrm{m}}$, which is near to that of brittle silicate glasses, to 80 MPa $\sqrt{\mathrm{m}}$, which is closer to that of tough structural alloys, have been reported [11]. The fracture surface morphology of ductile metallic glasses is coarse, with deep vein patterns, whereas that of brittle metallic glasses shows quasi-cleavage features with much finer vein patterns [12]. This dual (ductile and brittle) nature of fracture processes in metallic glasses is not clearly understood. One of the reasons for the variability in the fracture toughness of metallic glasses is the nature of processes occurring near the crack tip such as crack branching and shear banding [13]. The fracture toughness of glassy polymers is also low and lies in the range 1–5 MPa $\sqrt{\mathrm{m}}$ [14]. In these materials, processes like crazing and shear banding occur near the crack tip which affect the fracture response [15–17]. It is important to note that all the fracture mechanisms mentioned above depend strongly on the features of the near-tip stress and deformation fields. These, in turn, are likely to be influenced by the mechanical characteristics of amorphous materials like internal friction, softening, plastic dilatation, etc.

Li and Pan [18] studied the mode I asymptotic, crack tip fields in pressure-sensitive dilatant materials under 2D plane strain conditions. Jeong et al. [17] constructed theoretical slip lines in front of a round notch tip. Subramanya et al. [19] performed a 3D finite element analysis of mode I crack tip fields under SSY conditions. It should be noted that all of these studies were carried out within the framework of the small strain Drucker–Prager yield criterion. Further, a power law hardening response and a constant dilatancy parameter were assumed. However, as discussed earlier, the mechanical response of amorphous materials undergoing inhomogeneous plastic flow by shear banding is better described by a constitutive model such as that proposed by AS [2], which incorporates the Mohr–Coulomb yield criterion, a variable dilatancy parameter and dilatation induced softening. Indeed, AS [2,20] demonstrated that their model can accurately represent overall features such as load versus displacement response, as well as details of shear band formation during the deformation of metallic glasses in a variety of situations such as indentation and strip bending. It should be noted that a finite deformation analysis of crack tip fields in glassy polymers was conducted by Basu and Van der Giessen [15] using a totally different constitutive model that incorporates softening as well as orientation hardening [21]. However, this model is not based on Coulomb yield theory and also does not effectively represent pressure dependence of yielding.

In this work, a detailed finite element investigation of crack tip fields in amorphous plastic solids under mode I, plane strain, SSY conditions is carried out. The constitutive model proposed by AS [2] is used. The influence of friction parameter and flow softening on the plastic zone, stress and deformation fields and notch opening profiles are studied. In order to gain insight into the near-tip processes like shear banding and crack branching, plastic slip line fields and possible brittle crack trajectories around the notch root are generated. Further, the localization of plastic strain into discrete shear bands is simulated numerically by employing a statistical distribution of cohesion. It is found that a higher value of the friction parameter leads to a larger plastic zone and higher plastic strain level ahead of the notch tip, but leads to a substantial decrease in the opening stress. The propensity for localization of plastic strain into shear bands increases with friction parameter and is promoted by softening. The simulated brittle crack trajectories and shear band patterns match qualitatively with those observed in experiments reported in the literature.

3. Material model

The constitutive equations employed in this study are based on the finite deformation, Mohr–Coulomb type model proposed recently by AS [2]. In this model, a multiplicative decomposition of the deformation gradient into elastic and plastic parts is assumed as

$$\boldsymbol{F} = \boldsymbol{F}^{\mathrm{e}}\boldsymbol{F}^{\mathrm{p}} \tag{1}$$

The elastic part of the deformation is assumed to be small and the relationship between the principal Kirchhoff stresses and the principal logarithmic elastic strains is taken to be governed by the isotropic Hooke's law [22].

Following AS [2], it is assumed that plastic flow occurs by shearing accompanied by dilatation relative to some slip systems. For an isotropic material, there are no preferred directions other than the principal directions of stress (denoted by unit vectors $\boldsymbol{n}_1$, $\boldsymbol{n}_2$ and $\boldsymbol{n}_3$). Accordingly, six potential slip systems are defined relative to these principal directions, with a conjugate pair lying in each of the three planes formed by $(\boldsymbol{n}_1,\boldsymbol{n}_3)$, $(\boldsymbol{n}_1,\boldsymbol{n}_2)$ and $(\boldsymbol{n}_2,\boldsymbol{n}_3)$. In each of these planes, the slip systems are oriented such that the slip directions, represented by unit vectors $\boldsymbol{s}^{(\alpha)}$ (where, α denotes the slip system number), make an angle of $\pm\{\frac{\pi}{4}+\frac{\phi}{2}\}$ (ϕ being the angle of internal friction), with the maximum principal stress direction in that plane. The resolved shear stresses and compressive normal tractions on these potential slip systems are defined as

$$\tau^{(\alpha)} = \boldsymbol{s}^{(\alpha)}\cdot\boldsymbol{\tau}\boldsymbol{m}^{(\alpha)} \quad \text{and} \quad \sigma^{(\alpha)} = -\boldsymbol{m}^{(\alpha)}\cdot\boldsymbol{\tau}\boldsymbol{m}^{(\alpha)}, \quad \alpha\in\{1,2,\ldots,6\}$$

respectively, where $\boldsymbol{m}^{(\alpha)}$ is the unit slip plane normal for the αth slip system and $\boldsymbol{\tau}$ is the Kirchhoff stress. It can be shown that conjugate slip systems are equivalent to each other in the sense that they have equal resolved shear stresses and compressive normal tractions and thus, as seen from Eq. (3) below, develop equal slip rates.

The flow rule is written for the plastic part of the spatial velocity gradient similar to AS [2] as

$$\boldsymbol{l}^{\mathrm{p}} = \sum_{\alpha=1}^{6}\dot{v}^{(\alpha)}[(\boldsymbol{s}^{(\alpha)}\otimes\boldsymbol{m}^{(\alpha)}) + \beta(\boldsymbol{m}^{(\alpha)}\otimes\boldsymbol{m}^{(\alpha)})], \quad \dot{v}^{(\alpha)}\geqslant 0, \tag{2}$$

where, $\dot{v}^{(\alpha)}$ is the plastic shearing rate and β is the dilatancy function. On examining the above equation, it can be seen that this flow rule accounts for plastic shearing accompanied by dilatancy. The viscoplastic law for $\dot{v}^{(\alpha)}$ is taken to be

$$\dot{v}^{(\alpha)} = \dot{v}_0\left\{\frac{\tau^{(\alpha)}}{c+\mu\sigma^{(\alpha)}}\right\}^{1/m}\geqslant 0, \tag{3}$$

where, $\dot{v}_0$ is a reference plastic shearing rate and $m>0$ is the strain rate sensitivity parameter. The model becomes rate-independent in the limit as $m\to 0$. Further, $\mu=\tan\phi$ is the friction parameter and c is a stress-like internal variable called the cohesion which represents the yield strength in pure shear. It must be noted that $\beta=\mu$ corresponds to the associated flow rule. The dilatancy parameter β is assumed to be an exponential function of the plastic volumetric strain η as

$$\beta = \hat{\beta}(\eta) = \frac{g_0}{(e-1)}\left\{e^{\left(1-\frac{\eta}{\eta_{\mathrm{cv}}}\right)}-1\right\}, \tag{4}$$

so that it varies smoothly from g_0 to 0 as η changes from 0 to η_{cv}.

The evolution of local free volume of amorphous materials governs their plastic deformation [3,24]. As assumed by AS [2], the change in free volume of an amorphous material, from its virgin state, is associated with the plastic volumetric strain η, which is defined as $\eta=\ln(J^{\mathrm{p}})$, where $J^{\mathrm{p}}=\det(\boldsymbol{F}^{\mathrm{p}})$. Thus, the evolution of η is governed by the relation

$$\dot{\eta} = tr(\boldsymbol{l}^{\mathrm{p}}) = \beta\sum_{\alpha=1}^{6}\dot{v}^{(\alpha)}. \tag{5}$$

The cohesion c is assumed to vary smoothly with η according to the relation

$$c = c_{\mathrm{cv}} + \frac{b}{(e-1)}\left\{e^{\left(1-\frac{\eta}{\eta_{\mathrm{cv}}}\right)}-1\right\}. \tag{6}$$

From Eqs. (4)–(6), it can be seen that during the initial stages of plastic flow from a virgin state, η will increase monotonically and later saturate to an equilibrium level of η_{cv}, while the cohesion c will decrease smoothly from an initial value of $c_0=(b+c_{\mathrm{cv}})$ to an equilibrium value c_{cv}. The above model has been implemented in the general purpose nonlinear finite element code ABAQUS/Standard [25] by writing a user material subroutine UMAT. The integration of the constitutive equations is carried out using a fully implicit backward Euler approach [23].

The objective for the most part of this work is to study the effects of different material parameters on mode I crack tip fields under small scale yielding conditions by assuming an uniform value of the initial cohesion c_0 for the entire domain. However, in Section 6, the initial cohesion value is statistically distributed among the elements to numerically simulate strain localization behavior observed in amorphous metals.

4. Modeling and analysis aspects

4.1. Modeling details

A 2D plane strain boundary layer (SSY) formulation is used in the present study. For this purpose, a large circular domain containing a notch along one of its radii is considered (see Fig. 1a). The radius of the outer boundary (R_0) is chosen to be 400 times the initial notch root diameter b_0, so that the plastic zone is well contained within the boundary. In the undeformed configuration, the center of curvature O of the notch coincides with the center of the circular domain. A set of cartesian coordinates (X_1,X_2) is established with origin at O (see Fig. 1b). Due to symmetry arising because of mode I loading, only the upper-half plane is modeled with finite elements, as shown in Fig. 1a. Appropriate symmetry conditions are imposed on the line ahead of the notch tip and traction-free boundary conditions are assumed on the notch surface. The mesh employed in the analysis is well refined near the notch tip, with 16 elements placed along the semi-circumference of the notch (see Fig. 1b), in order to accurately capture the steep strain gradients and notch blunting. The size of the smallest element in the radial direction is about $1.4\times10^{-4}R_0$. The mesh comprises of a total of 3352 isoparametric quadrilateral elements and 3463 nodes.

The in-plane displacement components based on the leading term of the mode I elastic crack tip field [26] are prescribed on the outer boundary of the domain. The loading is applied in steps by gradually increasing the mode I

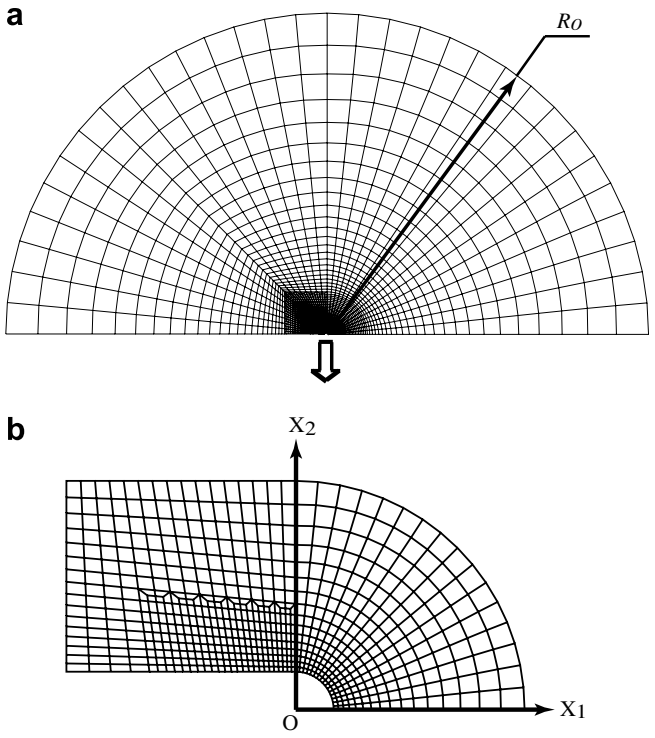

Fig. 1. The finite element mesh used in the simulations showing (a) the full domain that was modeled and (b) enlarged view of the region near the notch tip.

stress intensity factor K_I. In order to alleviate mesh locking effects due to near-plastic incompressibility, the hybrid element formulation available in ABAQUS [25] is employed in the simulations.

4.2. Choice of material parameters

In order to understand how the constitutive behavior influences the crack tip fields in amorphous plastic solids, a parametric study is conducted. A total of four sets of material combinations are considered, as listed in Table 1. These sets differ mainly in material parameters μ and b which govern the frictional response as well as pressure sensitivity of yielding and softening respectively. The chosen values of these parameters given in Table 1 are representative of different amorphous plastic solids such as metallic glasses and glassy polymers [4,7,8].

In all cases, the values of E/c_0 and Poisson's ratio are taken to be 108.5 and 0.36 respectively [11]. The present study is restricted to nearly rate-independent material response by assuming a small value of 0.02 for the strain rate sensitivity exponent m. The stress variations are presented in terms of Cauchy stress components normalized by the initial value of the cohesion c_0, which is a common stress-like quantity for all cases. It must be noted that material combination A (see Table 1) represents a Tresca-type yield behavior, whereas B and C are typical of an amorphous metal response with an increasing friction parameter μ. They were chosen so that a comparison between them brings out the effect of μ on the crack tip fields. The material combination D involves plastic dilatation but exhibits no softening after the initial yielding (i.e. it is elastic–perfectly plastic).

Table 1
Material combinations considered in the numerical simulations

Material combination	E/c_0	ν	μ	g_0	b/c_0
A	108.5	0.36	0.00	0.4	0.085
B	108.5	0.36	0.05	0.4	0.085
C	108.5	0.36	0.15	0.4	0.085
D	108.5	0.36	0.15	0.4	0.000

5. Results and discussion

The results obtained from the numerical simulations are discussed in this section.

5.1. Effect of friction parameter

The results of simulations for material combinations A, B and C (see Table 1) are compared in this subsection in order to understand the effect of varying the friction parameter (which, in turn, affects the pressure sensitivity of yielding) on the notch tip stress and deformation fields. Fig. 2 shows the plastic zones for three different values of friction parameter $\mu = 0$, 0.05 and 0.15, plotted in notch tip coordinates normalized by $(K_I/c_0)^2$. The plastic zone shape and size are expected to remain invariant with respect to these normalized coordinates, once the notch has blunted adequately. Here, the plastic zone boundary is defined by the curve where the maximum principal logarithmic plastic strain $\ln \lambda_1^p$ has a very small value of 0.001.

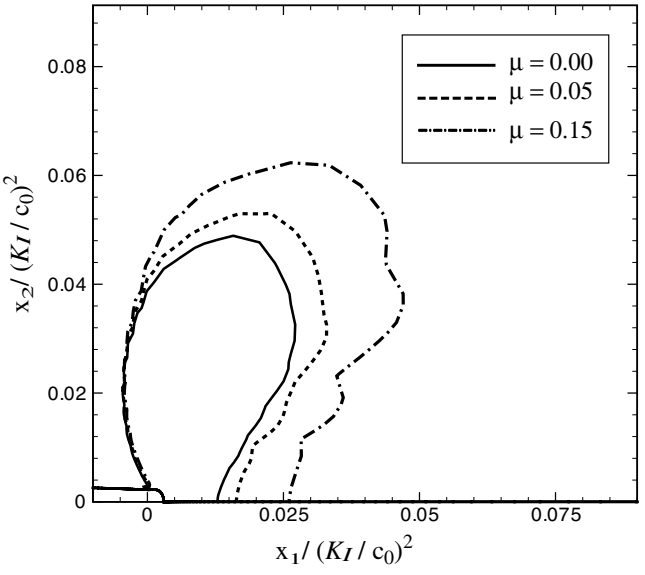

Fig. 2. Plastic zones plotted using normalized notch tip coordinates for different values of friction parameter.

It can be seen from Fig. 2 that the plastic zone size increases with μ. In particular, the extent of the plastic zone ahead of the notch tip doubles when μ is increased from 0 to 0.15. Further, the location of the maximum extent of plastic zone rotates forward with respect to the notch line and increases from 0.05 $(K_I/c_0)^2$ to 0.07 $(K_I/c_0)^2$. Xi et al. [27] have found a correlation showing direct correspondence between the fracture toughness and plastic process zone size for various metallic glasses. In view of this, the increased plastic zone size with μ suggests the enhanced fracture toughness of metallic glasses. It can be noticed from Fig. 2 that the propensity for a serrated plastic zone boundary increases with μ. This could be interpreted as a tendency to form the shear bands which have been observed in experiments [13] on amorphous metals (see also Section 6). It must be noted that metallic glasses have extremely high yield strength and low to moderate fracture toughness values [11], resulting in small plastic zone sizes in an absolute sense.

Fig. 3 shows the effect of varying the friction parameter μ on the distribution of the opening stress, normalized by the initial cohesion c_0, ahead of the notch tip. Here, the radial distance r is measured from the notch tip in the undeformed configuration and is normalized by (J/c_0), where c_0 is the yield strength in pure shear and J is the energy release rate. For small scale yielding conditions, the J integral is calculated from K_I using the relation $J = K_I^2(1-\nu^2)/E$. It can be seen from Fig. 3 that an increase in μ leads to a dramatic drop in $\sigma_{\theta\theta}$ ahead of the notch tip. The peak stress drops by about 27% with an increase in μ from 0 to 0.15, accompanied by a shift in the radial location from the notch tip at which it occurs, from 1.25 to 2.3 J/c_0. The reduction in $\sigma_{\theta\theta}$ with increasing μ is significant for $r/(J/c_0) < 3$, beyond which it tends to diminish. A similar trend can be seen in the radial distribution of hydrostatic stress, σ_h, ahead of the notch tip (see Fig. 4a). The peak value of σ_h drops by about 21% with an increase in μ from 0 to 0.15. Fig. 4b shows the radial distribution of normalized hydrostatic stress at $\theta = 45°$. Here, the angle θ is measured from the line ahead of the notch tip and centered at the notch tip in the undeformed configuration. It can be seen that higher μ results in a significant and uniform drop (by about 18%) in σ_h up to fairly large radial distances $(r/(J/c_0) \leqslant 5)$ from the notch tip.

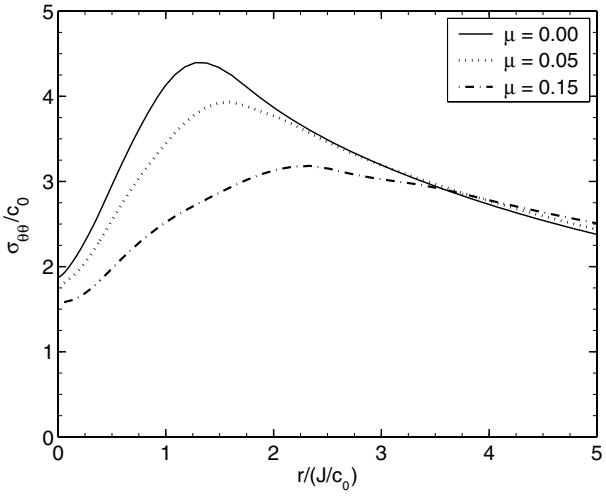

Fig. 3. Radial distribution of normalized opening stress at $\theta = 0°$ for different values of friction parameter.

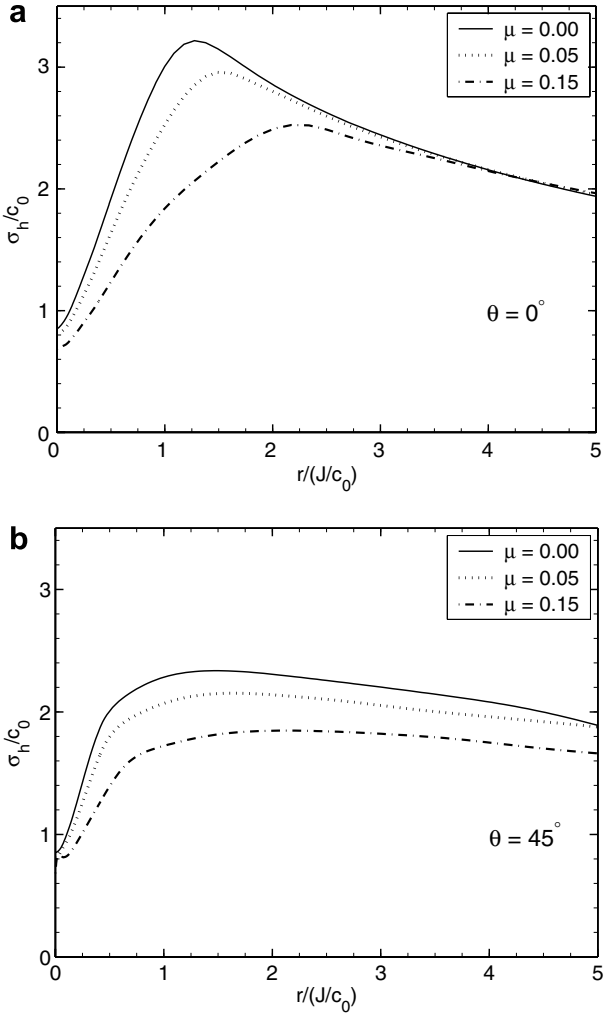

Fig. 4. Radial distribution of normalized hydrostatic stress at (a) $\theta = 0°$ and (b) $\theta = 45°$ for different values of friction parameter.

The above trends are qualitatively similar to those reported by Li and Pan [18] and Subramanya et al. [19] on the role of pressure sensitivity index from small strain analysis of crack tip fields in materials obeying the Drucker–Prager yield condition. By contrast, the present analysis is based on a Mohr–Coulomb type plasticity model that includes the effect of the third invariant J_3 of the deviatoric stress (see Section 3) and also incorporates finite geometry changes. Flores and Dauskardt [28] have shown, from their experimental results, that failure in a Zr-based bulk metallic glass is associated with a critical tensile hydrostatic stress. In view of this, the decrease in the opening stress and hydrostatic stress levels near the notch tip with increasing μ

suggests a reduced tendency to brittle cracking or increased resistance to fracture.

In Figs. 5a–d, the angular distributions of normalized radial, tangential, shear and hydrostatic stresses around the notch tip are displayed at $r/(J/c_0) = 1.5$, for three different values of μ. It can be observed from Fig. 5a that a higher μ leads to a uniform drop in σ_{rr} at all angles around the notch tip. Also, Fig. 5b shows that there is a dramatic decrease in $\sigma_{\theta\theta}$ at $\theta = 0°$ which diminishes with θ. This drop in $\sigma_{\theta\theta}$ is noticeable in the angular range $\theta \leqslant 75°$. The effect of increase in μ on $\sigma_{r\theta}$ is similar. It is interesting to note from Figs. 5a and b that, as μ increases, the difference $(\sigma_{\theta\theta} - \sigma_{rr})$ in the region ahead of the notch tip diminishes. This implies that the stress state ahead of the notch tends towards pure hydrostatic tension as μ increases even though the level of σ_h itself drops (see Fig. 5d). This could have important implications on the fracture behavior of the material. For example, the shape assumed by a circular void as it grows in the vicinity of a notch tip (i.e. whether it would remain circular or become oblate or prolate) depends on the nature of the stress state [29,30].

Fig. 6 shows the angular distribution of $\ln \lambda_1^p$ at $r/(J/c_0) = 1.5$. It can be seen that at angles $\theta \leqslant 90°$ the plastic strain level is strongly enhanced with increasing μ. Thus, the peak plastic strain increases by about 17.5% with a change in μ from 0 to 0.15 and is accompanied by a shift in its angular location towards the front of the notch tip. As the level of μ increases, many distinct serrations in the near-tip angular distribution of plastic strain can be observed in the forward sector ahead of the notch tip (up to about $\theta = 90°$). This corroborates with similar features perceived on the leading boundary of the plastic zone in Fig. 2. As already mentioned, it suggests a tendency for plastic strains to localize into discrete shear bands, which have been observed in experiments on both metallic glasses and amorphous polymers [13,17]. This issue will be taken up in subsequent sections.

It is interesting to compare the near-tip angular distribution of plastic strain shown in Fig. 6 with that reported in

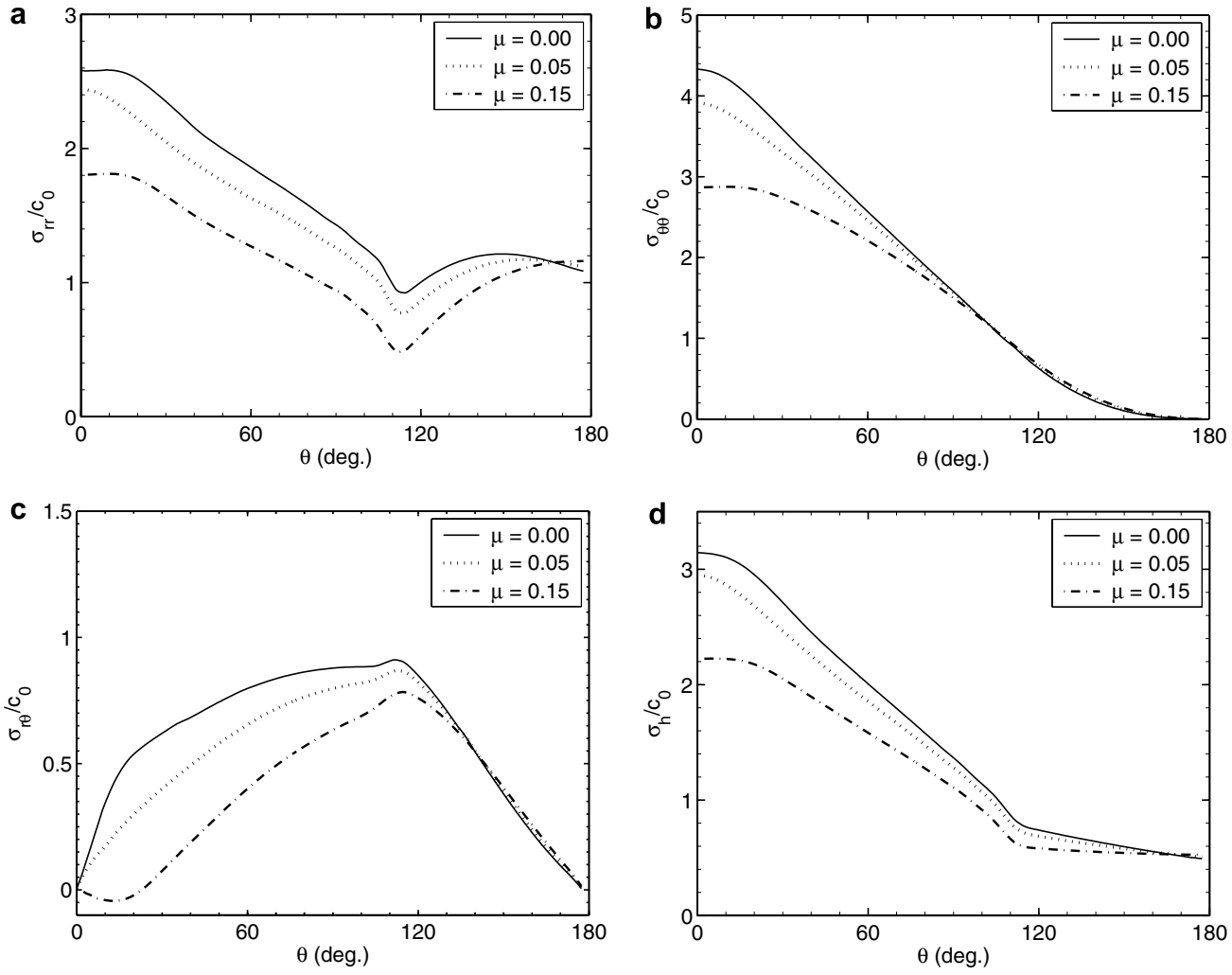

Fig. 5. Angular distributions of (a) radial, (b) tangential, (c) shear and (d) hydrostatic stresses normalized by c_0 around the notch tip at $r/(J/c_0) = 1.5$ for different values of friction parameter.

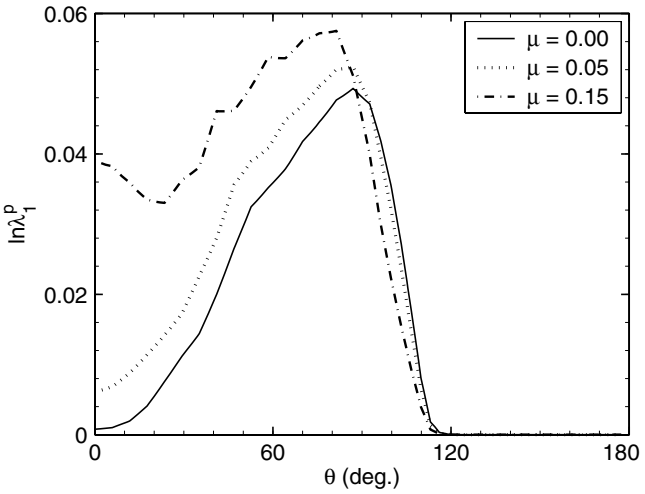

Fig. 6. Comparison of angular distribution of maximum principal logarithmic plastic strain at $r/(J/c_0) = 1.5$ for different values of friction parameter.

Ref. [19] from 3D, small strain analysis using the Drucker–Prager model in the mid-plane of a plate. Subramanya et al.'s results show more pronounced elevation in the peak plastic strain with pressure sensitivity index. The peak plastic strain in their plots occurs at a value of θ between 75° and 90°, which is similar to the curves presented in Fig. 6. However, since their computations are based on a small strain formulation and pertain to a sharp crack (i.e. ignoring blunting effects), very little plastic strain develops directly ahead of the tip, irrespective of the pressure sensitivity index. By contrast, the present results show a larger accumulation of plastic strain in the region ahead of the tip, especially with an increase in the friction parameter μ (see Fig. 6). This leads to an appreciable growth in the plastic zone size ahead of the notch tip, as observed from Fig. 2.

In Fig. 7, the notch opening profiles at a fixed level of normalized energy release rate, $J/(c_0 b_0) = 7.22$, pertaining to three different values of μ are compared. The distances are normalized by the initial notch root diameter b_0. All three cases show significant blunting of the notch by a factor of three to four owing to strong influence of plastic deformation. It can be observed from this figure that the notch opening profile is enhanced with increasing μ. Also, a prominent hump can be observed in the notch profile, especially for high μ, which is characteristic of non-hardening materials having a high yield strain.

In Fig. 8, the notch opening displacement $(b - b_0)$ normalized by b_0 is plotted against the normalized energy release rate $J/(c_0 b_0)$. Here, b is the current notch width calculated at the points which are located above and below the center of curvature of the notch in the undeformed configuration. It can be observed from this figure that in all cases there is an almost linear relation between notch opening displacement and energy release rate J. Also, as already noted, the notch opening enhances with μ at a given level of J. It is well known that the crack tip opening displacement scales with J where the scaling factor depends on the strain hardening exponent and initial yield strain [31]. The present results suggest that for amorphous plastic solids, it also depends on the friction parameter μ. Thus, the ratio $(b - b_0)/(J/c_0)$, calculated from the curves presented in Fig. 8 for cases A and C increases from 0.42 to 0.52 as μ changes from 0 to 0.15. The larger notch opening displacement with increase in μ corroborates with the enhancement in the near-tip plastic strain as well as the normalized plastic zone size with increase in friction parameter.

5.2. Effect of softening

In this section, comparison of results for material combinations C (which shows softening behavior) and D (which exhibits elastic–perfectly plastic response) is presented in order to understand the influence of softening response on the notch tip stress and deformation fields. It is found that softening leads to a decrease in all stress components around the notch tip. For example, in Fig. 9 the

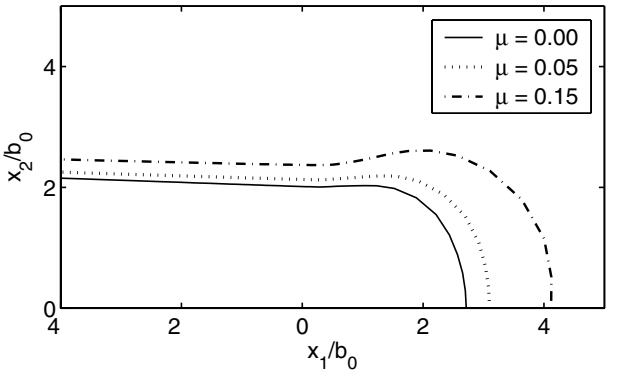

Fig. 7. Notch opening profiles corresponding to $J/(c_0 b_0) = 7.22$ for different values of friction parameter.

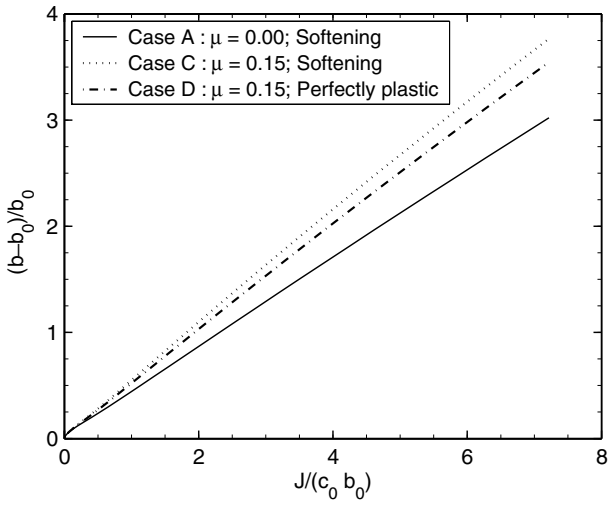

Fig. 8. Variation of notch opening displacement with respect to $J/(c_0 b_0)$ for different material combinations.

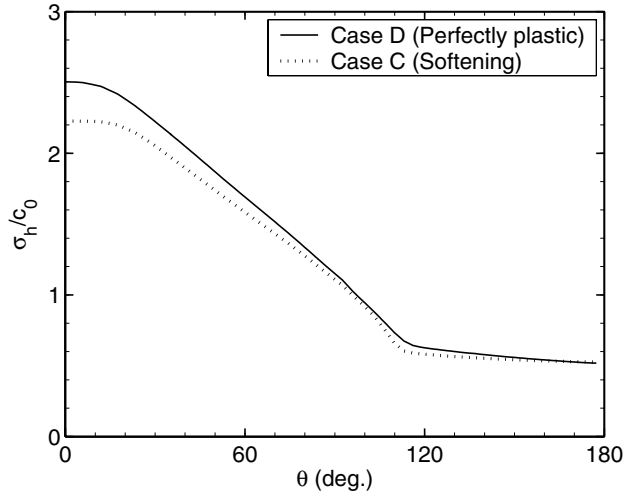

Fig. 9. Angular distribution of normalized hydrostatic stress around the notch tip at $r/(J/c_0) = 1.5$ for material combinations C and D.

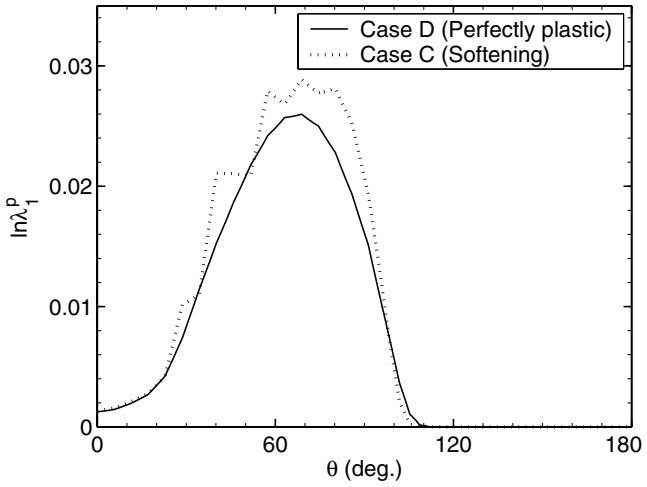

Fig. 10. Angular distribution of $\ln\lambda_1^p$ at $r/(J/c_0) = 3$ for material combinations C and D.

angular distribution of normalized hydrostatic stress around the notch tip at $r/(J/c_0) = 1.5$ is displayed for the two cases. It can be seen from this figure that softening leads to a perceptible reduction in σ_h near the notch tip at all angles $\theta \leqslant 75°$. In particular, the hydrostatic stress ahead of the notch tip ($\theta = 0°$) decreases by about 12% due to presence of softening.

Fig. 10 shows the angular distribution of $\ln\lambda_1^p$ at $r/(J/c_0) = 3$ for material combinations C and D. It can be observed from this figure that, although the angular location of the peak plastic strain is unaffected by softening, its magnitude is increased. In particular, the plastic strain levels around the notch tip for $30° \leqslant \theta \leqslant 90°$ are considerably enhanced (by up to about 11%). Another striking feature of this figure is the appearance of sharp serrations in the angular distribution of plastic strain when the material exhibits softening. It must be noted that a similar trend is seen in Fig. 6 with increase in μ. This suggests that the propensity for localization of plastic strain into discrete shear bands increases with μ and is also enhanced by the presence of softening in the material response.

The effect of softening on the evolution of notch opening displacement with the normalized energy release rate can be seen from Fig. 8 by comparing the curves pertaining to cases C and D. It can be observed from this figure that the notch opening displacement varies linearly with J and that softening results in about 7% higher notch blunting at any J. This result is consistent with the fact that softening promotes the plastic strain levels around the notch tip, as seen in Fig. 10.

5.3. Slip line fields around the notch

Strain softening exhibited by amorphous materials such as metallic glasses and glassy polymers, is invariably accompanied by localization of plastic strain into shear bands [13,17]. Crack propagation upon accumulation of a critical amount of plastic strain after continued shearing along these discrete bands is believed to be one of the failure modes in metallic glasses [32]. Hence, in order to gain a better understanding of such a ductile failure mechanism, the plastic slip line fields around the notch are studied in this subsection.

Fig. 11a shows the slip line fields prevailing around the blunted notch for material combination C corresponding to normalized energy release rate of $J/(c_0 b_0) = 0.8$. In this figure, the slip lines generated using the stress fields obtained from the finite element solution are plotted in the deformed configuration and the distances are normalized by the initial notch root diameter b_0. Here, and in similar plots shown subsequently, the trajectories in the lower half are obtained from those in the upper-half by reflection about $x_2 = 0$ line for complete visualization. Under 2D plane strain conditions, there are two slip systems in the x_1–x_2 plane which are symmetrically disposed at angles of $\pm\left\{\frac{\pi}{4} + \frac{\phi}{2}\right\}$ about the maximum in-plane principal stress direction, where $\phi = \tan^{-1}\mu$ (see Section 3). The two families of slip lines, indicated by solid and dashed-dotted lines in Fig. 11a, represent the trajectories of these directions in the x_1–x_2 plane. In this figure, the slip line network is enclosed within a curve (indicated by the dotted line) which represents the elastic–plastic boundary. For clarity, an enlarged view of the slip line network close to the notch and entirely inside the zone of large plastic deformation is shown in Fig. 11b.

The included angle between the two families of slip lines emanating from the notch surface in Figs. 11a and b is 81.5°, unlike isotropic pressure insensitive plastic solids, where the slip lines under plane strain conditions coincide with the maximum shear directions and are thus orthogonal. The slip line fields for a rigid-perfectly plastic, von Mises material [26] and a pressure-sensitive dilatant material obeying the Drucker–Prager yield condition [18] predict intense straining above and below a sharp crack

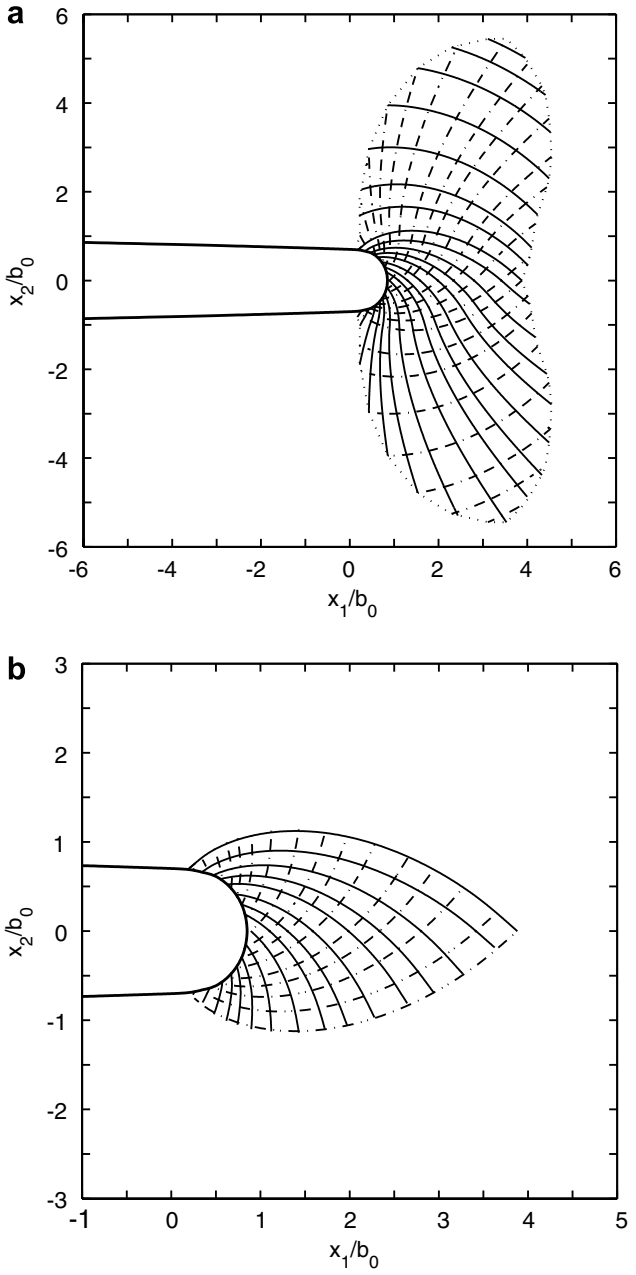

Fig. 11. Slip line fields around the blunted notch for material combination C corresponding to $J/(c_0 b_0) = 0.8$. (a) Full field view and (b) enlarged view near the notch tip.

tip and not directly in front of it. In the latter, the slip line grid is formed by two non-orthogonal families of characteristic lines and the angular extents of the constant stress sectors in front of the tip and adjacent to the crack face vary with the pressure sensitivity index of the material. By contrast, the slip line field in Fig. 11a suggests large plastic strains immediately ahead of the blunting notch tip due to large geometry changes. It resembles the theoretical slip line field around a notch constructed by Jeong et al. [17] for a pressure sensitive and dilatant material (see Fig. 6 of their paper). Also, the dashed-dotted family of slip lines in the upper half and the solid family of slip lines in the lower half of Fig. 11a look similar to the shear band patterns observed around a crack in experiments conducted by Flores and Dauskardt [13] using SEN(T), Vitreloy 1 metallic glass fracture specimen (see Fig. 3 of their paper).

5.4. Brittle crack trajectories in front of the notch

Under macroscopic tension, amorphous materials like bulk metallic glasses and glassy polymers such as PMMA are quasi-brittle because they exhibit very little plastic deformation. Hence, it is important to examine the probable crack paths if failure in these materials occurs due to brittle fracture. Since fracture in a brittle solid is controlled by the maximum normal tensile stress acting on the fracture plane, it is reasonable to assume that crack growth should be orthogonal to the direction of most tensile principal stress [33]. Such trajectories have been successfully employed to trace the paths of contact-induced transverse cracks in brittle coatings on soft substrates by Lee et al. [34]. The above trajectories corresponding to material combination C are plotted in Fig. 12 at a value of $J/(c_0 b_0) = 0.2$ when the notch blunting is not substantial ($b/b_0 = 1.13$).

From Fig. 12, it can be seen that the crack trajectories become asymptotic to the $x_2 = 0$ line, which is a principal stress direction owing to mode I symmetry. Also, planes tangent to the notch surface, which is traction-free, represent principal planes containing the maximum principal stress direction. Thus, the crack trajectories originate orthogonally from the notch surface. Another interesting feature that can be observed is that the trajectories, after

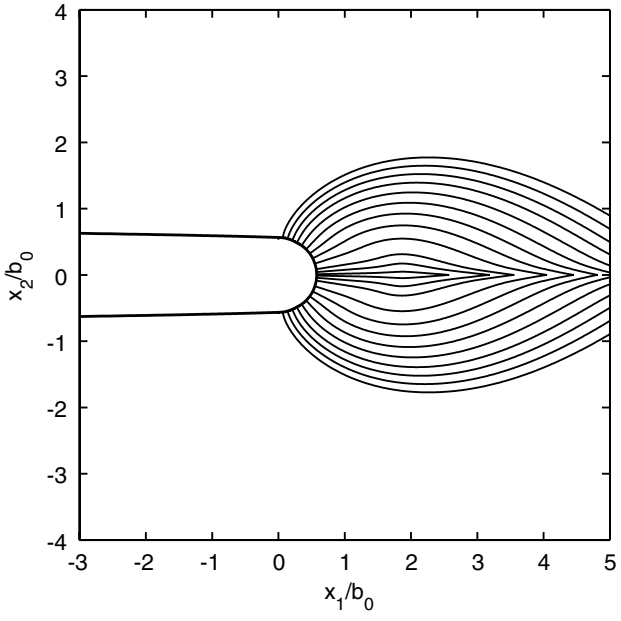

Fig. 12. Trajectories of normal to the maximum principal stress direction in front of the notch, for material combination C corresponding to $J/(c_0 b_0) = 0.2$.

starting orthogonal to the notch surface, rise and reach a peak height at a distance of about 1.5 times the current notch width in front of the notch tip and later become asymptotic to the $x_2 = 0$ line. These trajectories resemble the crack traces observed in front of a notch tip in experiments conducted on a Zr-based metallic glass by Lowhaphandu and Lewandowski [35] (see Fig. 3 of their paper) using three-point bend specimens and by Fujita et al. [36] using compact tension specimens. From these experimental pictures and the nature of crack trajectories in Fig. 12, one is led to conclude the following about the brittle fracture mechanism in metallic glasses. Several microcracks simultaneously originate orthogonally from the notch surface. With increasing load, these microcracks propagate along trajectories similar to those shown in Fig. 12. At some stage, they merge together at a finite distance in front of the notch tip to form a single macroscopic mode I crack which subsequently causes brittle catastrophic failure of the specimen.

6. Simulation of shear band pattern around the notch

All the results discussed in the previous section were obtained by assuming the same initial value of the cohesion for the entire domain. However, at temperatures well below their glass transition temperature, amorphous solids such as metallic glasses exhibit inhomogeneous deformation when subjected to high stresses [37]. The inhomogeneous deformation in metallic glasses is characterized by an increase in local free volume at some discrete locations followed by localization of plastic strain in those regions resulting in the formation of narrow shear bands. In order to numerically simulate this inhomogeneous deformation behavior at the continuum scale, the initial value of the cohesion is statistically varied among all elements in the mesh following AS [2]. This leads to an inhomogeneously distributed plastic volumetric strain (which, in the present constitutive model, is considered to be equivalent to the change in free volume from the virgin state) and provides a sufficient number of nucleation sites for the shear bands to form (see AS [2]).

In this section, the results of a simulation in which the initial value of the cohesion is varied among all elements using a normal distribution with standard deviation of 3% of the mean value c_0 are presented. The other properties used in this simulation correspond to material combination C (see Table 1). In Fig. 13, contour plots of maximum principal logarithmic plastic strain, $\ln \lambda_1^p$, near the notch are displayed in the deformed configuration corresponding to different stages of loading.

Figs. 13a–c show the development of shear bands near the notch at normalized energy release rate $J/(c_0 b_0)$ of 0.2, 0.45 and 0.8, respectively. In Fig. 13d, an enlarged view of the region around the notch of Fig. 13c is shown for clarity. In these figures, the lowest contour of $\ln \lambda_1^p = 0.001$ gives a representation of the elastic–plastic boundary. Thus, the plastic zone which is confined to the region just in front of the notch at $J/(c_0 b_0) = 0.2$ (see Fig. 13a) grows with increasing load and assumes a close to self-similar shape at $J/(c_0 b_0) = 0.8$ (see Fig. 13c), which roughly corresponds to that depicted in Fig. 2 for $\mu = 0.15$. It should be noted from Figs. 13a–c that plastic deformation progresses by way of formation of new shear bands and propagation of existing ones. The shear bands resemble discrete fingers projecting out from the notch, leading to the elastic–plastic boundary having a serrated nature (see Figs. 13b and c). This feature of the elastic–plastic boundary can also be observed to a lesser extent in Fig. 2. Such plastic zones caused by inhomogeneous flow along discrete bands have also been reported by Lai and Van der Giessen [21] (see Fig. 8 of their paper) employing an entirely different constitutive model for amorphous polymers which exhibits strain softening.

At a low value of $J/(c_0 b_0) = 0.2$, a dense network of multiple shear bands of both families can be seen in front of the notch in Fig. 13a. The two families of shear bands close to the notch tip can also be clearly seen in Fig. 13d at a higher load level with an included angle of less that 90° between them. This pattern of shear bands is similar to the slip line fields in front of the notch predicted from the simulation with uniform initial cohesion (Fig. 11b). It also resembles that observed in experiments on amorphous polymers reported by Jeong et al. [17] (see Figs. 2 and 3 of their paper). It can be noticed that the level of plastic strain is greatest in shear bands which are very near to the notch surface and diminishes rapidly with increasing distance from it. The intense plastic straining in a few bands may cause ductile shear failure along these bands, leading to the formation of macroscopic cracks [32]. Finally, it should be noted that the shear bands away from the notch root in the outer reaches of the plastic zone (see Fig. 13c) are similar to those observed experimentally for Vitreloy 1 metallic glass by Flores and Dauskardt [13] (see Fig. 3 of their paper).

An interesting feature that can be observed from Fig. 13d is the blunting of the notch surface into a shape with several vertices when the initial cohesion is statistically distributed. These vertices form at locations on the notch surface where the two families of shear bands intersect each other and may be interpreted as shear offsets or surface steps. Such waviness on the notch surface has also been reported by Lai and Van der Giessen [21] in their simulations for amorphous polymers. Finally, it should be mentioned that, although there are qualitative similarities between the predictions of the present simulations and the experimental observations reported by Jeong et al. [17], as well as the above computational study [21], the role of progressive hardening at large plastic strains arising due to orientation of molecular chains in some polymers [38] has not been assessed in this work. This feature is considered in Refs. [15,21], wherein a different constitutive model based on statistical distribution of molecular chains is employed.

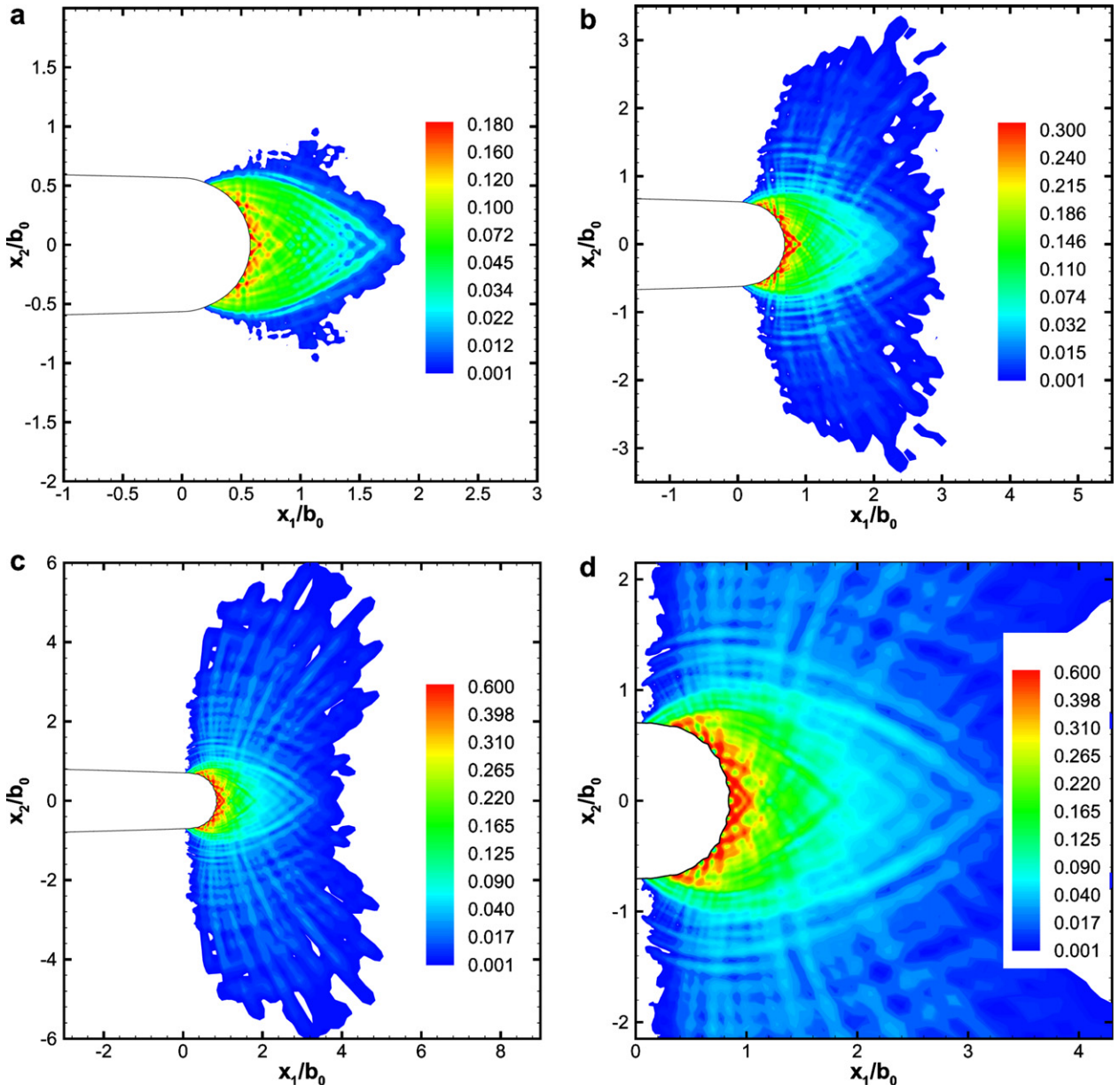

Fig. 13. Contours of maximum principal logarithmic plastic strain showing the development of shear bands for material combination C when the initial cohesion c_0 is statistically distributed over the mesh, corresponding to (a) $J/(c_0 b_0) = 0.2$, (b) $J/(c_0 b_0) = 0.45$, (c) $J/(c_0 b_0) = 0.8$. (d) Enlarged view of (c) near the notch tip.

7. Conclusions

In this work, a finite strain Mohr–Coulomb based constitutive model, with provision for discrete slip systems (defined locally with respect to the principal stress directions), was employed to study the notch tip stress and deformation fields in amorphous solids such as metallic glasses under mode I, plane strain, small scale yielding conditions. The following are some of the important conclusions that can be drawn from the simulations performed in this work.

An increase in the value of friction parameter μ increases the plastic zone size ahead of the notch tip and causes it to rotate forward. Also, the plastic zone boundary shows serrated features and the notch tip opening displacement is enhanced. A higher μ also leads to a severe decrease in opening stress ahead of the notch tip and a reduction in hydrostatic stress at all angles around the notch tip. On the other hand, it also results in a strong increase in the plastic strain accumulation ahead of the notch tip. These observations, in combination with the one-to-one correspondence between plastic zone size and toughness established earlier in metallic glasses [27], suggests that enhanced internal friction could lead to improved fracture toughness of the amorphous material. Although softening results in the reduction in the levels of all stress components,

it enhances the plastic strains around the notch, which is also reflected in the enlarged notch opening profile. The propensity for localization of plastic strain into discrete shear bands increases with μ and is further enhanced in the presence of softening.

The synthetic slip line field constructed around the blunted notch suggests large plastic strains immediately ahead of the notch tip and resembles that reported from experiments on an amorphous polymer [17]. The predicted brittle crack trajectories rise orthogonal to the notch surface and after reaching a peak height become asymptotic to the line directly ahead of the notch tip, which suggests coalescence of microcracks ahead of the notch tip as seen in experiments on metallic glasses [35,36]. The resulting shear band patterns generated from simulations with statistical distribution of initial cohesion are similar to the synthetic slip line field predicted from the stress distribution around the notch as well as to those observed in experiments [13,17].

In summary, the present numerical study on crack tip fields in amorphous materials such as metallic glasses and non-crystalline polymers suggests a competition between crack tip plasticity through shear banding and brittle fracture by microcracking. Higher friction parameter suppresses the latter by decreasing the opening stress levels near the notch tip. On the other hand, it promotes crack tip plasticity through shear banding. The discrete plastic zone in the form of shear bands, which is aided by softening, may increase the resistance to fracture by dissipation of energy in the shear bands. This is especially true if multiple shear bands form, each accommodating moderate plastic strains. Eventually, when extremely large plastic strains are accumulated into a few shear bands, ductile fracture may occur within them [32]. Also, the large plastic strains associated with higher μ could give rise to alternate ductile fracture mechanisms such as growth and coalescence of microvoids (e.g. around rubber particles in rubber modified epoxies) [29].

References

[1] Schuh CA, Hufnagel TC, Ramamurty U. Acta Mater 2007;55:4067.
[2] Anand L, Su C. J Mech Phys Solids 2005;53:1362.
[3] Bhowmick R, Raghavan R, Chattopadhyay K, Ramamurty U. Acta Mater 2006;54:4221.
[4] Quinson R, Perez J, Rink M, Pavan A. J Mater Sci 1997;32:1371.
[5] Heard HC, Cline CF. J Mater Sci 1980;15:1889.
[6] Bowden PB, Jukes JA. J Mater Sci 1972;7:52.
[7] Donovan PE. Acta Mater 1989;89:445.
[8] Lu J, Ravichandran G. J Mater Res 2003;18:2039.
[9] Patnaik MNM, Narasimhan R, Ramamurty U. Acta Mater 2004;52:3335.
[10] Lund AC, Schuh CA. Acta Mater 2003;51:5399.
[11] Lewandowski JJ, Wang WH, Greer AL. Phil Mag Lett 2005;85:77.
[12] Nagendra N, Ramamurty U, Goh TT, Li Y. Acta Mater 2000;48:2603.
[13] Flores KM, Dauskardt RH. Scripta Mater 1999;41:937.
[14] Kim BH, Joe CR, Otterson DM. Polym Test 1989;8:119.
[15] Basu S, Van der Giessen E. Int J Plasticity 2002;18:1395.
[16] Kambour RP. Macromolecular reviews. J Polym Sci 1973;7:1.
[17] Jeong HY, Li XW, Yee AF, Pan J. Mech Mater 1994;19:29.
[18] Li FZ, Pan J. Trans ASME: J Appl Mech 1990;57:40.
[19] Subramanya HY, Viswanath S, Narasimhan R. Int J Solids Struct 2007;44:1893.
[20] Anand L. Su C. Acta Mater 2006;54:179.
[21] Lai J, Van der Giessen E. Mech Mater 1997;25:183.
[22] Anand L. J Appl Mech 1979;46:78.
[23] Armero F. Elastoplastic and viscoplastic deformations in solids and structure. In: Stein E, Borst R, Hughes TJR, editors. Encyclopedia of computational mechanics solids and structures, vol. 2. John Wiley & Sons, Ltd.; 2004 [Chapter 7].
[24] Flores KM, Suh D, Howell R, Asoka-Kumar P, Sterne PA, Dauskardt RH. Mater Trans 2001;42:619.
[25] ABAQUS. Reference manuals, version 6.5. RI, USA: Hibbitt, Karlsson and Sorensen, Inc.; 2004.
[26] Rice JR. Mathematical analysis in the mechanics of fracture. In: Liebowitz H, editor. Fracture, vol. II. Academic Press; 1968.
[27] Xi XK, Zhao DQ, Pan MX, Wang WH, Wu Y, Lewandowski JJ. Phys Rev Lett 2005;94:125510.
[28] Flores KM, Dauskardt RH. Acta Mater 2001;49:2527.
[29] Chew HB, Guo TF, Cheng L. Int J Solids Struct 2006;43:6380.
[30] Subramanya HY, Viswanath S, Narasimhan R. Eng Fract Mech, in press. doi:10.1016/j.engfracmech.2007.04.022.
[31] Shih CF. J Mech Phys Solids 1981;29:305.
[32] Conner RD, Johnson WL, Paton NE, Nix WD. J Appl Phys 2003;94:904.
[33] Frank FC, Lawn BR. Proc Roy Soc Lond 1967;A299:291.
[34] Lee KS, Wuttiphan S, Hu XZ, Lee SK, Lawn BR. J Am Ceram Soc 1998;81:571.
[35] Lowhaphandu P, Lewandowski JJ. Scripta Mater 1998;38:1811.
[36] Fujita K, Okamotob A, Nishiyama N, Yokoyamad Y, Kimura H, Inoue A. J Alloy Compd 2007;434–435:22.
[37] Spaepen F. Acta Mater 1977;25:407.
[38] Hope PS, Duckett RA, Ward IM. J Appl Poly Sci 1980;25:1373.